iScience

Article

Predictive value of machine learning model based on CT values for urinary tract infection stones

Graphical abstract

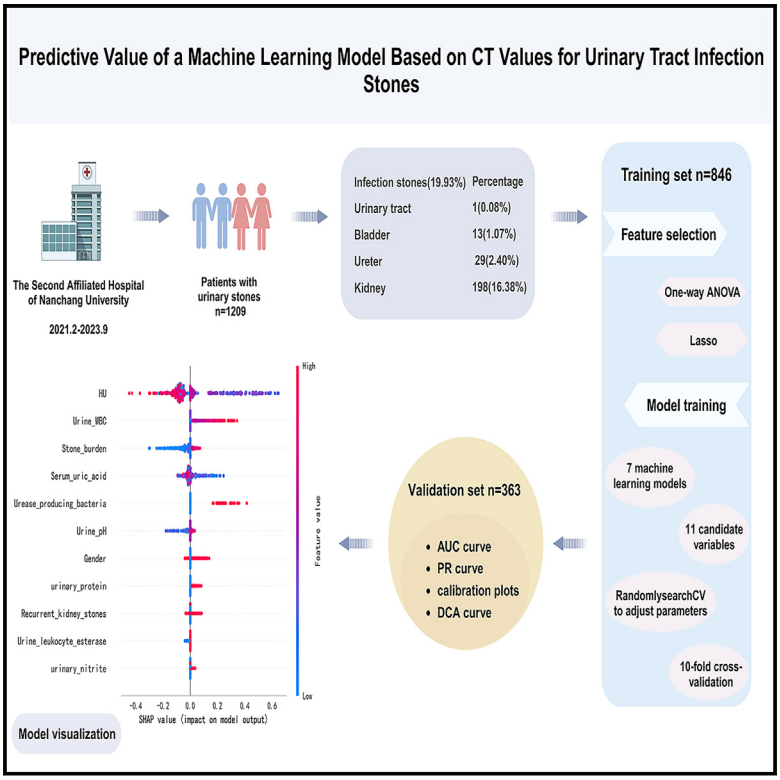

Highlights

- Machine learning model for predicting urinary tract infection stones
- The model we developed demonstrates good predictive performance
- Analyzed the clinical characteristics of infection stones in the Chinese population

Authors

Jiaxin Li, Yao Du, Gaoming Huang, ..., Jinghui Zhong, Xiaoqing Xi, Yawei Huang

Correspondence

xixiaoqing500@sina.com (X.X.), 273895819@qq.com (Y.H.)

In brief

Nephrology; Bioinformatics

Li et al., 2024, iScience *27*, 110843
December 20, 2024
https://doi.org/10.1016/j.isci.2024.110843

CellPress

iScience

CellPress
OPEN ACCESS

Article

Predictive value of machine learning model based on CT values for urinary tract infection stones

Jiaxin Li,[1,4] Yao Du,[2,4] Gaoming Huang,[1] Chiyu Zhang,[1] Zhenfeng Ye,[1] Jinghui Zhong,[3] Xiaoqing Xi,[1,*] and Yawei Huang[1,5,*]

[1]Department of Urology, The Second Affiliated Hospital, Jiangxi Medical College, Nanchang University, Nanchang 330006, China
[2]Department of Cardiovascular Medicine, The Second Affiliated Hospital, Jiangxi Medical College, Nanchang University, Nanchang 330006, China
[3]Department of Neurology, Centre for Leading Medicine and Advanced Technologies of IHM, The First Affiliated Hospital of USTC, Division of Life Sciences and Medicine, University of Science and Technology of China, Hefei, Anhui 230001, China
[4]These authors contributed equally
[5]Lead contact
*Correspondence: xixiaoqing500@sina.com (X.X.), 273895819@qq.com (Y.H.)
https://doi.org/10.1016/j.isci.2024.110843

SUMMARY

Preoperative diagnosis of infection stones presents a significant clinical challenge. We developed a machine learning model to predict urinary infection stones using computed tomography (CT) values, enabling *in vivo* preoperative identification. In this study, we included 1209 patients who underwent urinary lithotripsy at our hospital. Seven machine learning algorithms along with eleven preoperative variables were used to construct the prediction model. Subsequently, model performance was evaluated by calculating AUC and AUPR for subjects in the validation set. On the validation set, all seven machine learning models demonstrated strong discrimination (AUC: 0.687–0.947). Additionally, the XGBoost model was identified as the optimal model significantly outperforming the traditional LR model. Taken together, the XGBoost model is the first machine learning model for preoperative prediction of infection stones based on CT values. It can rapidly and accurately identify infection stones *in vitro*, providing valuable guidance for urologists in managing these stones.

INTRODUCTION

Urological stones are increasingly prevalent in the field of urology. Epidemiological analyses indicate a rise in their prevalence in China, from 4% to 6.4% in recent years, with notable regional differences. The southern region shows a higher prevalence (11.6%) compared to the northern (7.2%).[1] Infection stones, a specific type of urinary tract stone, are composed of minerals such as struvite, carbonate apatite, and ammonium urate. Their etiology and formation mechanisms are complex, with a strong association with urinary tract infections caused by urease-producing bacteria, including *Proteus mirabilis*, *Klebsiella pneumoniae*, *Pseudomonas aeruginosa*, Staphylococcus, and Morganella.[2] Clinically, infection stones exhibit distinctive features, such as rapid growth, high recurrence rates, and a propensity for serious complications.[3] Consequently, managing patients with infection stones presents significant challenges in urolithiasis, representing a particularly demanding subset. The close association between infection stones and urease-producing bacteria increases the risk of postoperative complications, such as uroseptic shock and systemic inflammatory response syndrome.[4]

Effective management of infection stones involves a comprehensive array of therapeutic strategies, including pre- and postoperative antibiotics, meticulous surgical removal of stone fragments, litholytic therapy, urine acidification, and urease inhibitors.[5] Regardless of the treatment approach, early and accurate identification of infection stones is essential. Currently, precise determination of stone composition is limited to *in vitro* analysis using infrared spectroscopy, presenting a significant diagnostic constraint in clinical practice. Preoperative diagnosis of infection stones heavily relies on recognized risk factors for infection, including advanced age, female gender, cerebrovascular disease, abnormal urinary tract anatomy, and diabetes mellitus.[6–9]

The diagnosis of urinary stones relies on CT examination due to its superior sensitivity, specificity, and safety compared to other imaging modalities. CT scans are more efficient, do not necessitate contrast media, and are unaffected by renal function and intestinal gas interference. Spiral CT is commonly utilized in clinical settings for urolithiasis diagnosis, with urinary stones typically manifesting as dense calcified shadows on CT images, although stone density may vary among different types. The measurement of CT values can aid in the preliminary assessment

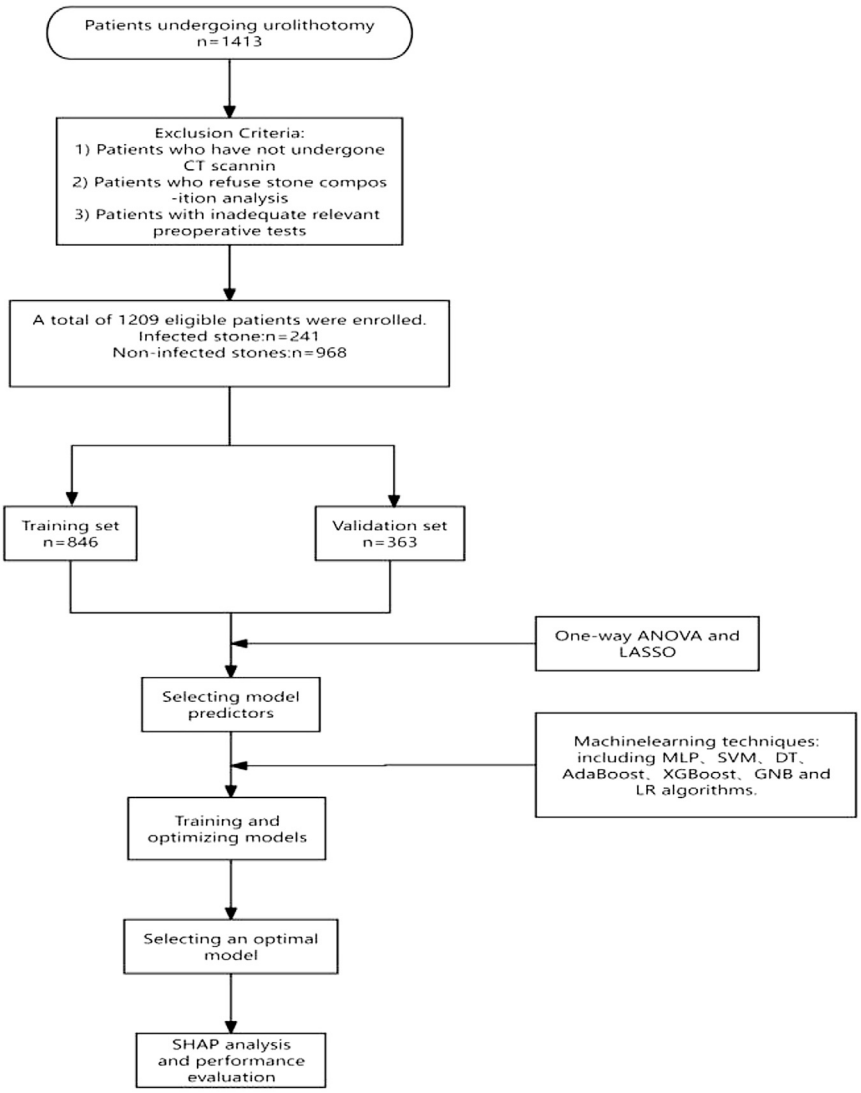

Figure 1. Machine learning model building flowchart

of stone composition.[10] However, Marchini et al.[11] caution against solely relying on CT values for precise predictions of infection stone composition. Consequently, this clinical study aims to develop a comprehensive predictive model based on CT values to facilitate the preoperative identification of infection stones *in vivo*.

Machine learning models utilize data and statistical techniques to enable computer systems to predict outcomes and make decisions, which is particularly prevalent in the medical field. The Multilayer Perceptron (MLP) is a neural network algorithm with hidden layers comprising nodes that undergo multilayer nonlinear transformations to abstract and classify input data.[12] The Support Vector Machine (SVM) is a binary classification method that considers each feature as a dataset dimension to segment the dataset effectively based on the classification of interest.[13] The Decision Tree (DT) algorithm facilitates classification and regression tasks by recursively partitioning datasets into a tree structure, enabling sample classification or prediction.[14] Adaptive Boosting (AdaBoost) is an iterative training methodology that enhances the performance of weak classifiers by amalgamating them into a robust classifier.[15] Gaussian Naive Bayes (GNB) is rooted in probabilistic principles and Gaussian distributions, providing a classification methodology based on its probabilistic foundation.[16] Extreme Gradient Boosting (XGBoost), similar to AdaBoost, iteratively trains decision tree models to refine model performance by progressively correcting errors. This study constructed and selected an optimal machine learning model using these seven algorithms and preoperative variables such as CT values. Urologists can tailor treatment strategies by identifying patients at high risk of developing infection stones. These results highlight the essential role of machine learning in enhancing clinical decision-making processes in urology.

RESULTS

Study population

This study enrolled 1209 eligible patients, and the study flow chart is shown in Figure 1. The stone composition and CT values are detailed in Table 1. Most of the patients' urinary stones were composed of calcium oxalate, totaling 808 (66.83%) cases. There were 241 (19.9%) cases of infection stones, with only 48 (3.97%) identified as pure infection stones. Most infection stones consisted of struvite or carbonate apatite mixed with calcium oxalate. There were 6 cases (0.4%) of calcium hydrogen phosphate stones. Cystine stones were excluded due to their scarcity. Among the infection stones, the CT values were (666.43 ± 128.46) HU for pure ammonium magnesium hexaphosphate struvite and (731.72 ± 161.56) HU for pure carbapatite. The CT value for mixed infection stones primarily composed of struvite was (902.03 ± 165.34) HU, while for those dominated by carbonate apatite, it was (889.51 ± 171.64) HU. The CT value for stones containing both carbapatite and struvite was (708.41 ± 83.62) HU. Among the non-infection stones, the CT value of pure calcium oxalate stones was (1346.05 ± 175.02) HU, and the CT value of mixed non-infection stones with calcium oxalate predominance was (1241.36 ± 219.86) HU. The CT value of pure uric acid stones was (426.58 ± 103.97) HU, while the CT value of uric acid + calcium oxalate stones was (526.49 ± 202.45) HU.

Table 1. Distribution of urinary stone composition and CT values

Parameter	Patients,n (%)	Range	Mean ± SD
Predominantly infection stones	241 (19.93)	**308.67∼1346.43**	**855.68±177.20**
Pure struvite	13 (1.07)	308.67–812.49	666.43 ± 128.46
Mixed-predominantly struvite	68(5.62)	637.85–1328.43	902.03 ± 165.34
Pure carbapatite	10(0.83)	637.85–1328.43	731.72 ± 161.56
Mixed-predominantly carbapatite	125 (10.34)	506.30–1346.43	889.51 ± 171.64
struvite +carbapatite	25(2.07)	554.36–886.54	708.41 ± 83.62
Predominantly noninfection stones	968 (80.07)	**165.58∼1843.23**	**1156.49±354.07**
Pure calcium oxalate	308 (25.48)	789.56–1796.66	1346.05 ± 175.02
Mixed-predominantly calcium oxalate	500 (41.36)	568.90–1843.23	1241.36 ± 219.86
Pure uric acid	50 (4.14)	165.58–738.88	426.58 ± 103.97
Mixed-predominantly uric acid	104 (8.60)	267.52–1461.28	526.49 ± 202.45
Pure calcium phosphate	6 (0.50)	1098.50–1608.35	1354.75 ± 162.42

Simple infection stones are defined as having ≥95% of that infection stone component, and mixed infection stones are defined as having ≥50% of that infection stone component. Mixed-predominantly struvite Includes struvite + calcium oxalate, struvite + carbapatite + calcium oxalate. Mixed-predominantly carbapatite Includes carbapatite + calcium oxalate, carbapatite + struvite + calcium oxalate. Mixed-predominantly calcium oxalate Includes calcium oxalate + struvite/carbapatite. Mixed - predominantly uric acid stones including uric acid + calcium oxalate.

The frequency of pathogens detected in positive urine cultures is illustrated in Figure S3. Among patients with infection stones, *P. mirabilis* was the predominant pathogen (n = 43), followed by *Escherichia coli* (n = 31) and *K. pneumoniae* (n = 15). For non-infection stones, *E. coli* was the most frequently identified pathogen (n = 113), followed by *Enterococcus faecalis* (n = 25) and Streptococcus agalactiae (n = 18). The main urease-producing organisms included *P. mirabilis*, *K. pneumoniae*, *P. aeruginosa*, Staphylococcus spp., and Morganella spp.

One-way analysis of variance and lasso regression

A total of 1209 case samples were randomly divided into a training set (70%) and a validation set (30%). The prevalence of infection stones in the overall sample (19.93%) did not significantly differ from that in the training set (19.6%) and the validation set (20.7%). Except for urinary RBC, no significant differences were found in any variables between the training and validation sets($P > 0.05$), as shown in Table S1.

Univariate analysis of the training set is presented in Table 2. A higher proportion of female patients than male patients presented with infection stones (M/F = 0.73 $p < 0.05$). Additionally, other variables associated with infection stones included body mass index (p = 0.023), history of recurrent stones (p = 0.01), recurrent renal stones ($p < 0.01$), number of stones ($p < 0.01$), stone location ($p < 0.01$), stone load ($p < 0.$ 01), CT value ($p < 0.01$), urine PH ($p < 0.01$), urine nitrite positivity ($p < 0.01$), urine protein positivity ($p < 0.01$), urine occult blood positivity (p = 0.01), urine leukocyte esterase positivity ($p < 0.$ 01), urine WBC positivity ($p < 0.01$), urine culture positivity ($p < 0.01$), urease producing bacteria positivity ($p < 0.01$), urine turbidity (p = 0.01), serum uric acid ($p < 0.01$) and serum neutrophil percentage (p = 0.012). Variables with $p < 0.05$ in the one-way analysis of the training set were included in the Lasso regression analysis, resulting in the selection of 11 variables for constructing the predictive model: gender, stone burden, history of recurrent kidney stones, HU, urine pH, urinary nitrite, urinary protein, urine leukocyte esterase, urine WBC, urease-producing bacteria, and serum uric acid (Figures 2A and 2B).

Model performance

We selected parameter values for training each model and conducted a 10-fold cross-validation to assess their performance using various criteria. Tables S2 and 3 present the area under the curve (AUC) values, accuracy, specificity, sensitivity, positive predictive value (PPV), negative predictive value (NPV), and F1 scores of each model within the training and validation sets, respectively. The receiver operating characteristic (ROC) curves depicting the performance of different models are illustrated in Figures 3A and 3B. The AUC values of the different models in the validation set were as follows: XGBoost 0.947 (95% CI 0.921-0. 973), LR 0.906 (95% CI 0.869–0.943), AdaBoost 0.937 (95% CI 0.905–0.969), DT 0.903 (95% CI 0.863–0.944), GNB 0.909 (95% CI 0.877–0.941), SVM 0.752 (95% CI 0.702–0.803) and MLP 0.687 (95% CI 0.625–0.750). Except for the DT, MLP and SVM models, the AdaBoost, XGBoost, and GNB models demonstrated superior performance to the traditional LR models. The accuracy values of the seven machine learning models ranged from 0.64 to 0.896, sensitivity values ranged from 0.635 to 0.915, and specificity values ranged from 0.697 to 0.872. Furthermore, XGBoost exhibited the highest area under the precision-recall curve (AUPR) in both the training and validation sets (Figures 3C and 3D). Based on these results, particularly considering the sensitivity, specificity, and AUPR values, XGBoost is the optimal model choice [AUC: 0.947 (95% CI 0.921–0.973), accuracy 0.896 (95% CI 0.887–0.905), sensitivity 0.901 (95% CI 0.872–0.931), specificity 0.869 (0.837–0.901), AUPR 0.957 (0.944–0.971)].

The SHAP to model interpretation

The Shapley Additive exPlanations (SHAP) method was used to assess the significance of each variable in predicting outcomes in the XGBoost machine learning model (Figures 4A and 4B).

Table 2. Univariate analysis between infection and noninfection stone groups in the training and validation sets

	Training set			validation set		
Characteristics	Non-infection stones (*n* = 680)	infection stones (*n* = 166)	p	Non-infection stones (*n* = 288)	Infection stones (*n* = 75)	p
Gender (Female)(%)	194 (28.5)	98 (59.0)	**<0.001**	85 (29.5)	41 (54.7)	<0.001
Age (years),(mean (SD))	52.87 (13.50)	50.73(14.64)	0.073	52.06 (13.33)	51.72(15.37)	0.848
BMI (kg/m^2),(mean (SD))	24.05 (3.41)	23.39 (3.14)	**0.023**	23.96 (3.65)	23.94 (3.52)	0.969
Diabete,(n%)	81 (11.9)	27 (16.3)	0.168	30 (10.4)	17 (22.7)	0.009
Hypertension,(n%)	194 (28.5)	40 (24.1)	0.295	77 (26.7)	16 (21.3)	0.42
Recurrence,(n%)	179 (26.3)	66 (39.8)	**0.001**	84 (29.2)	22 (29.3)	0.999
Number of stones(mean(SD))	2.69 (1.62)	3.3 (2.18)	**<0.001**	2.61 (1.49)	3.21 (2.26)	0.006
Stone burden (mm^2)(mean (SD))	218.60(274.78)	430.14(552.20)	**<0.001**	204.99(247.84)	404.82(504.64)	<0.001
HU (mean (SD))	1144.94(359.9)	857.78(180.68)	**<0.001**	1183.74(338.96)	851.03(170.34)	<0.001
Recurrent kidney stones,(n%)	122 (17.9)	60 (36.1)	**<0.001**	56 (19.4)	22 (29.3)	0.089
Stone location (n%)			**<0.001**			0.004
Bladder	34 (5.0)	11 (6.6)		19 (6.6)	2 (2.7)	
Ureter	190 (27.9)	20 (12.0)		85 (29.5)	9 (12.0)	
Kidney	454 (66.8)	134 (80.7)		182 (63.2)	64 (85.3)	
Urinary tract	2 (0.3)	1 (0.6)		2 (0.7)	0 (0.0)	
Degree of hydronephrosis(n%)			0.294			0.001
None	92 (13.5)	20 (12.0)		46 (16.0)	2 (2.7)	
Light	267 (39.3)	54 (32.5)		111 (38.5)	23 (30.7)	
Medium	196 (28.8)	55 (33.1)		93 (32.3)	31 (41.3)	
Heavy	125 (18.4)	37 (22.3)		38 (13.2)	19 (25.3)	
Urine pH (mean (SD))	5.98 (0.59)	6.50 (0.65)	**<0.001**	6.01 (0.62)	6.53 (0.65)	<0.001
Urine specifc gravity(mean(SD))	1.02 (0.01)	1.02 (0.01)	0.085	1.02 (0.01)	1.02 (0.01)	0.136
Positive urinary nitrite,(n%)	55 (8.1)	44 (26.5)	**<0.001**	19 (6.6)	17 (22.7)	<0.001
Positive urinary glucose,(n%)	36 (5.3)	9 (5.4)	0.999	19 (6.6)	5 (6.7)	0.999
Positive urinary protein,(n%)	233 (34.3)	91 (54.8)	**<0.001**	97 (33.7)	46 (61.3)	<0.001
Positive urine occult blood,(n%)	571 (84.0)	156 (94.0)	**0.001**	226 (78.5)	75 (100.0)	<0.001
Positive ULE,(n%)	428 (62.9)	139 (83.7)	**<0.001**	177 (61.5)	65 (86.7)	<0.001
Positive urine_turbidity,(n%)	252 (37.1)	85 (51.2)	**0.001**	100 (34.7)	35 (46.7)	0.076
Urine RBC (mean (SD))	2.20 (1.68)	2.39 (1.72)	0.183	1.89 (1.51)	2.32 (1.49)	0.027
Urine WBC (mean (SD))	2.04 (1.40)	2.93 (1.45)	**<0.001**	2.05 (1.41)	3.05 (1.58)	<0.001
Positive urine culture,(n%)	158 (23.2)	89 (53.6)	**<0.001**	63 (21.9)	36 (48.0)	<0.001
Positive urease producing bacteria(n%)	25 (3.7)	49 (29.5)	**<0.001**	11 (3.8)	25 (33.3)	<0.001
Serum uric acid(umol/L),(mean (SD))	395.61(104.55)	317.61 (84.85)	**<0.001**	388.22 (101.34)	323.99 (84.28)	<0.001
BUN (mmol/L),(mean (SD))	100.91 (65.63)	105.74 (65.40)	0.395	96.97 (57.80)	95.68 (43.87)	0.857
Blood calcium (mmol/L),(mean (SD))	2.39 (0.13)	2.39 (0.16)	0.725	2.38 (0.13)	2.38 (0.16)	0.997
Leukocytes counts (mean (SD))	7.07 (2.31)	7.41 (2.54)	0.096	7.08 (2.89)	7.08 (2.72)	0.999
Neutrophils (mean (SD))	64.85 (10.25)	67.12 (10.90)	**0.012**	65.22 (10.19)	66.32 (9.65)	0.397

The bold numbers indicate statistically significant values. BMI, body mass index; BUN, blood urea nitrogen; urine RBC, urine red blood cells; SD, standard deviation; ULE, urine leukocyte esterase; urine WBC, urine white blood cells; HU, Hounsfield unit, CT value.

Figure 4A displays 11 important features of the XGBoost model, where each line on the vertical axis represents a feature, and the horizontal axis represents the SHAP values (the distribution of the effect of features on the model output). Each dot on a feature line represents a sample, with red dots indicating higher feature values and blue dots indicating lower feature values. Factors such as moderate stone HU values, elevated urinary leukocytes, increased stone load, reduced blood uric acid, urinary urease-producing bacterial infections, heightened urinary pH, female gender, increased urinary proteins, recurrent stones, and positive urinary leukocyte esterase and urinary nitrites promote the development of infection stones. Figure 4B shows the mean

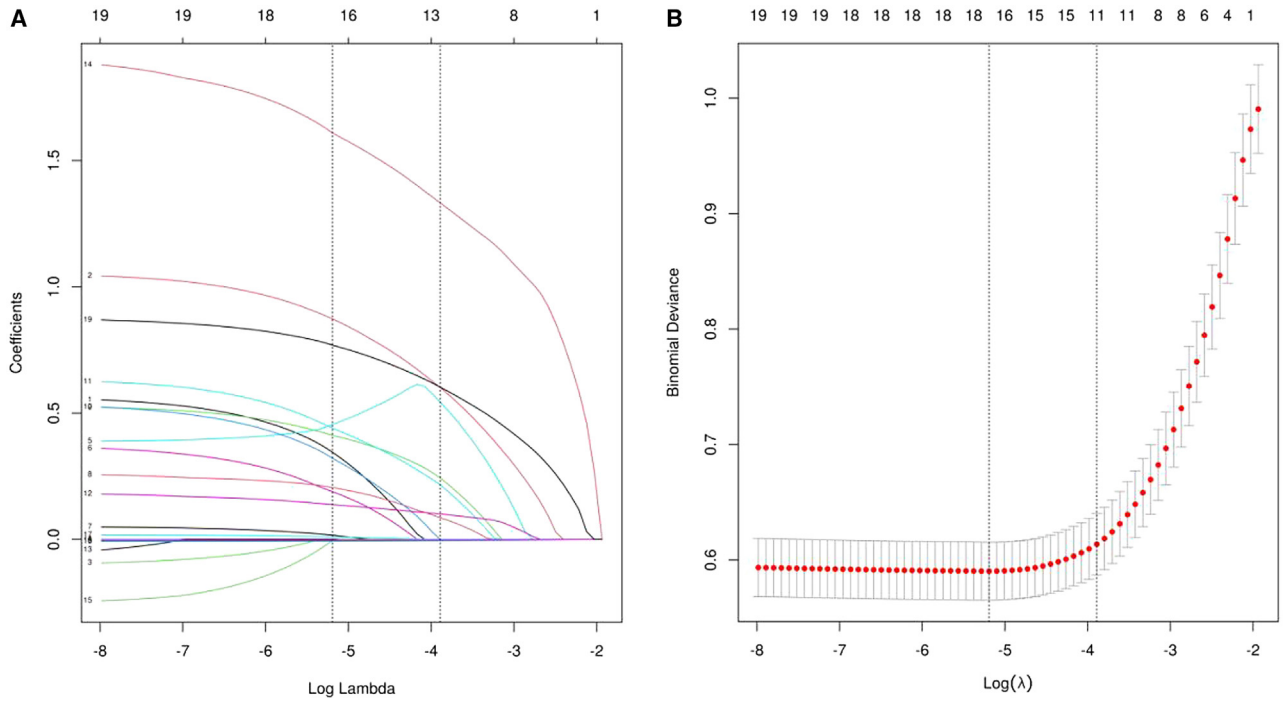

Figure 2. Use of lasso regression analysis for variable selection

(A) Vertical lines were drawn over selected values using 10-fold cross validation, where the best lambda produced 11 non-zero coefficients.

(B) Distribution of coefficients for 19 texture features extracted from the log (λ) sequence. Vertical dashed lines are drawn at the minimum mean square error (λ = 0.006) and the standard error of the minimum distance (λ = 0.02). optimal λ When the value is 0.02, our model selects 11variables: Gender, stone burden, Recurrent kidney stones, HU, Urine PH, Urinary protein, Urinary nitrite, Urine leukocyte esterase, Urine WBC, Urease producing bacteria, Serum uric acid.

absolute values of the SHAP values of the 11 features, indicating the importance of these features, with the horizontal axis representing the mean absolute SHAP values.

Model evaluation

In the XGBoost model, the DCA curves demonstrate a net benefit within the threshold probability range, indicating that utilizing the model for decision-making can yield greater benefits than the ''treat-all'' and ''treat-none'' approaches. These findings underscore the clinical value of the model, offering decision-makers valuable insights for informed decision-making. Moreover, the calibration curves exemplify the high accuracy and strong diagnostic performance of the XGBoost model within the cohort (Figures 5A and 5B).

DISCUSSION

The integration of machine learning algorithms into medical practice has witnessed a substantial increase in recent years, equipping clinicians with invaluable tools for swift and precise disease diagnosis and the customization of treatment protocols. This study developed and assessed seven distinct machine learning models, including XGBoost, Logistic Regression (LR), Adaptive Boost (AdaBoost), Decision Tree (DT), Gaussian Naive Bayes (GNB), Multilayer Perceptron (MLP), and Support Vector Machine (SVM), to discriminate between patients with infectious stones and those with non-infectious stones. The comprehensive analysis spanned a wide array of parameters, incorporating CT imaging features, demographic attributes, and urine culture findings. Among the seven machine learning models, XGBoost emerged as the optimal model, exhibiting superior performance[AUC: 0.947 (95% CI 0.921–0.973), accuracy 0.896 (95% CI 0.887–0.905), sensitivity 0.901 (95% CI 0.872–0.931), specificity 0.869 (0.837–0.901), AUPR 0.957 (0.944–0.971)]. The study utilized DCA and calibration curves to assess the effectiveness of the XGBoost model in predicting infection stones. Furthermore, the utilization of the SHAP method improved the predictive accuracy and interpretability of our model and provided insights into the relative significance of individual features in the prediction process. Significantly, our findings highlighted the significant role of Hounsfield Unit (HU) values among the features in improving the predictive accuracy of the model. The incorporation of conventional clinical parameters in our machine learning prediction model not only ensures accessibility and user-friendliness but also eliminates the need for complex technical requirements. Consequently, the model holds promise for widespread adoption in primary healthcare settings, offering considerable potential for enhancing clinical decision-making and patient care outcomes.

Infectious stones represent a distinct subtype of urinary tract stones, posing considerable challenges in urolithiasis management. Characterized by rapid growth, high recurrence rates, and a tendency for serious complications, infection stones can quickly assume staghorn-shaped formations, exacerbating

Table 3. Diagnostic performance of different machine models for infected stones in the validation set

MODEL	AUC (95% CI)	Accuracy (95% CI)	Sensitivity (95% CI)	Specificity (95% CI)	PPV (95% CI)	NPV (95% CI)	F1 (95% CI)	Cutoff (95%CI)
XGB	0.947(0.921–0.973)	0.896(0.887–0.905)	0.901(0.872–0.931)	0.869(0.837–0.901)	0.708(0.682–0.735)	0.953(0.945–0.960)	0.792(0.770–0.815)	0.295(0.261–0.329)
LR	0.906(0.869–0.943)	0.817(0.799–0.834)	0.853(0.828–0.878)	0.826(0.799–0.853)	0.535(0.503–0.567)	0.949(0.937–0.962)	0.656(0.631–0.681)	0.197(0.166–0.229)
ADB	0.937(0.905–0.969)	0.881(0.873–0.889)	0.901(0.873–0.930)	0.872(0.855–0.889)	0.65(0.624–0.677)	0.962(0.949–0.976)	0.754(0.737–0.770)	0.477(0.467–0.487)
DT	0.903(0.863–0.944)	0.851(0.837–0.865)	0.852(0.810–0.894)	0.844(0.812–0.876)	0.609(0.567–0.651)	0.943(0.932–0.955)	0.707(0.679–0.735)	0.244(0.209–0.279)
GNB	0.909(0.877–0.941)	0.805(0.790–0.820)	0.915(0.881–0.949)	0.8(0.777–0.823)	0.516(0.488–0.544)	0.965(0.954–0.976)	0.659(0.631–0.687)	0.026(0.018–0.034)
SVM	0.752(0.702–0.803)	0.725(0.562–0.888)	0.833(0.755–0.912)	0.703(0.497–0.910)	0.498(0.391–0.605)	0.922(0.892–0.953)	0.594(0.493–0.695)	0.637(0.506–0.768)
MLP	0.687(0.625–0.750)	0.64(0.579–0.702)	0.635(0.506–0.765)	0.697(0.608–0.786)	0.347(0.293–0.401)	0.896(0.876–0.917)	0.417(0.382–0.453)	0.289(0.244–0.334)

AUC, area under the receiver operating characteristic curve; XGBoost, Extreme Gradient Boosting; LR, logistic regression; ADB, AdaBoost, Adaptive Boost; DT, Decision Tree; GNB, Gaussian Naive Bayes; SVM, Support Vector Machine; MLP = Multilayer Perceptron; PPV, Positive predictive value; NPV, Negative predictive value.

clinical complexities.[17] If left untreated, these stones can result in severe complications such as renal pelvic necrosis, perinephric abscess formation, renal failure, and, in extreme cases, may require kidney removal or lead to fatality.[18] Recent studies have shown that patients with untreated staghorn stones have a 50% risk of kidney loss,[19] and the 15-year overall survival rate for patients with untreated infection stones is only 41%. Moreover, 30% of patients with untreated infection stones who do not undergo surgical intervention ultimately succumb to sepsis or renal failure.[20] Surgical treatment introduces a high risk of postoperative infectious complications. Previous literature has reported a sepsis rate of 0.3–9.3% after surgery for urinary tract stones,[21] while Liu et al.[22] noted a 19% incidence of postoperative septicemia in infection stones.

Accurate preoperative identification of these stone types is crucial for guiding appropriate treatment decisions in clinical practice. The most widely accepted treatment for infection stones is the complete surgical extraction of stone fragments, as any remaining fragments can form new infection stones.[23] Percutaneous nephrolithotomy is recommended for larger renal infection stones (>2 cm), while ureteroscopy and extracorporeal shock wave lithotripsy (SWL) are alternatives for stones <2 cm. Ureteroscopy and percutaneous nephrolithotripsy offer a higher stone clearance rate than ESWL.[24] Due to their relatively soft and friable nature compared to other urinary stones,[25] infection stones are more easily fragmented during surgical procedures. However, the substantial volume of stone debris produced during fragmentation may release infectious bacteria into the urinary tract, increasing the risk of re-infection and stone recurrence.[26] Therefore, in addition to surgery, the treatment of infection stones should incorporate preoperative and postoperative antibiotic regimens, urine acidification, and urease inhibitor supplementation to reduce the risk of recurrence and growth of infection stones.[27]

The initial step in managing infection stones entails the detection and identification of the stones. CT is a rapid and reliable method for detecting and precisely locating stones within the urinary tract. On CT scans, stones manifest as dense calcification shadows; however, the density of various stone types varies, resulting in differing CT values. For instance, typical struvite stones exhibit a density of 900 HU or lower on CT imaging.[28] Consistent with our research, the mean CT value of infection stones in our study was 855.68 ± 177.20 HU, while non-infection stones had a mean CT value of 1156.49 ± 354.07 HU, showing a significant difference ($p < 0.05$) (Table 1). However, there is an overlap in CT values between infection stones and other types of stones (e.g., calcium oxalate and uric acid stones), thereby limiting the utility of CT values alone in predicting infection stones.[11] Therefore, we constructed a comprehensive prediction model based on CT values to facilitate the preoperative identification of infection stones. Furthermore, CT scans indicated that infection stones are predominantly situated in the kidney, exhibiting a greater number and burden compared to non-infection stones (Table 2).

Urinary tract infections and metabolic disorders are the two main causes of urinary tract stone development.[29] Struvite stones are conventionally linked to urinary tract infections instigated by urease-producing bacteria.[30] A positive urine culture

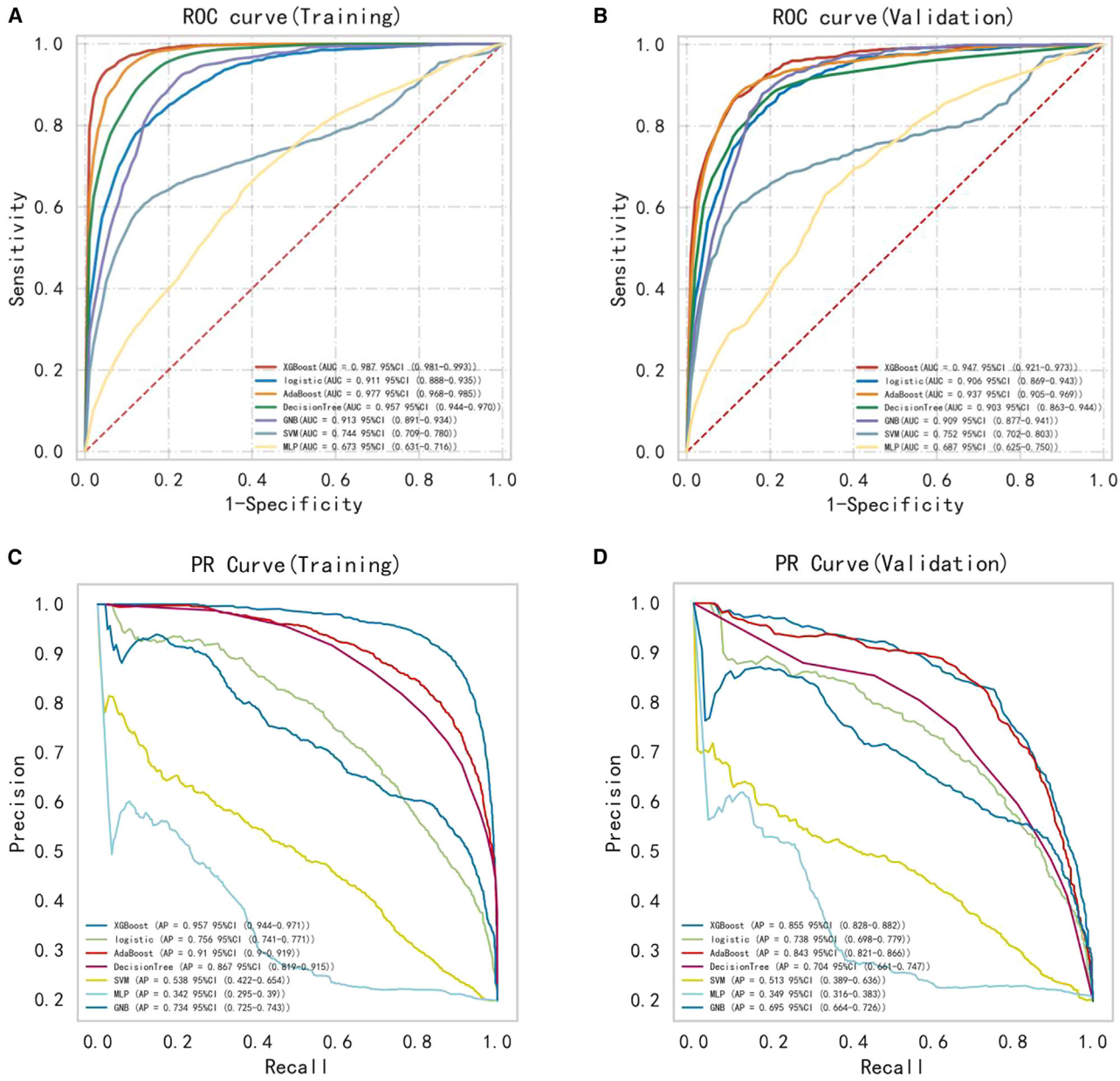

Figure 3. Comprehensive analysis of machine learning models in training and validation sets

(A) Training cohort ROC and AUC; (B) Validation cohort ROC and AUC.

(C) Training set PR curve and AP, and (D) validation set PR curve and AP. The y axis represents precision, and the x axis represents recall. If the PR curve of one model is completely covered by the PR curve of another model, it can be concluded that the latter is better than the former, and the higher the AP value, the better the model performance. The different colors in the image represent the corresponding models.

is considered a risk factor for infection stones,[31] and urease-producing bacteria in the urine culture suggests that the urinary stone might be an infection stone. This study identified positive urine culture and urease-producing bacterial infection as predictors of infection stones. However, the occurrence of urease-producing bacteria in infection stones was not notably high (30.71%) (Table 2), possibly due to the utilization of mid-stream urine for cultivation. Previous studies have underlined the inadequacy of urine culture as a precise method for pathogen identification in conditions linked with urinary tract infections.[32] To enhance accuracy, future strategies might involve direct culturing of stone samples or, when stone cultures are unavailable, obtaining urine specimens from the closest infection site, such as directly from the renal pelvis.[33]

Urease-producing bacteria synthesize urease, an enzyme that hydrolyzes urea in urine to generate carbon dioxide and ammonia. Consequently, NH_4+ and HCO_3- ions are produced, causing an increase in urine pH. When the pH of the urine exceeds certain

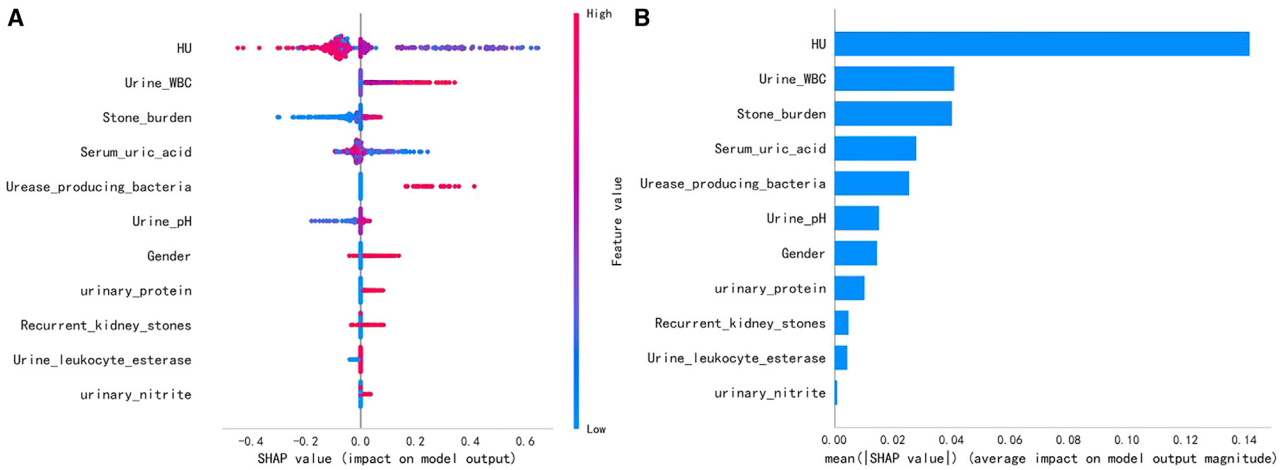

Figure 4. SHAP interprets the model

(A) The vertical axis ranks the features according to the sum of the SHAP values of the samples and the horizontal axis is the SHAP value. Each point represents a sample, with red points representing higher feature values and blue points representing lower feature values.

(B) Ranking of feature importance by mean(|SHAP value|). HU = Hounsfield unit = CT value. urine WBC = urine white blood cell. SHAP value = Shapley Additive exPlanations value.

thresholds, it promotes the gradual saturation of metal salts, leading to the crystallization of infectious stone components.[3] Carbonate apatite crystals precipitate when the pH exceeds 6.8, whereas struvite crystals form at pH > 7.2,[34] and carbonate apatite can form larger aggregates at high pH > 8.5.[35] Our study supports that an elevated urinary pH contributes to the precipitation of infection stones, consistent with the existing literature. The utilization of a comprehensive 24-h urinalysis is essential for the metabolic assessment of urinary stones and plays a pivotal role in developing our infection stones prediction model. Urinary pH, protein, nitrite, and leukocytes emerged as significant predictors through univariate analysis and lasso regression.

This study observed a higher prevalence of urinary stones in males and a greater incidence of infection stones in females (M/F = 0.73 $p < 0.05$) (Table 2). The increased susceptibility of women to develop infection stones may be attributed to the higher frequency of urinary tract infections and generally elevated urine pH levels in females.[36] Other factors, such as age, diabetes, and hyperuricemia, are also recognized as potential risk factors for infection stones.[29,37,38] However, our study did not identify a significant correlation between age, diabetes, and the occurrence of infection stones. Utilizing the SHAP method (Figure 4A), our analysis revealed that low blood uric acid levels could predispose individuals to infectious stone formation. Despite the higher susceptibility of diabetics to urinary tract infections, our findings did not show a significant association between diabetes and infection stone formation. A study[39] proposed that urinary glucose competitively inhibits uric acid reabsorption in diabetic patients, resulting in higher uric acid excretion. Additionally, insulin resistance in diabetics may alter urinary hydrolases, increase urine acidity, and decrease urinary pH, which may not be conducive to infection stone crystallization.

While previous research has explored machine learning models for infection stones,[40–42] it presents several advantages. Firstly, we possess a notably large sample size, the largest in the current literature. Secondly, our study incorporated CT imaging features of stones, and by applying the SHAP method, we have identified CT value as a critical predictor for infected stones. Subsequently, we developed seven machine learning models using lasso regression for variable selection. After analyzing the AUC and AUPR, we found that the XGBoost model outperformed the other models. The DCA and calibration curves of the XGBoost model were plotted to validate its robust diagnostic performance. While machine learning models demonstrate high accuracy, elucidating their decision-making processes comprehensively and transparently remains challenging. Hence, we applied the SHAP method to the XGBoost model to enhance interpretability and determine the importance of the modeled variables.

Our study has several limitations. First, it is a retrospective study conducted at a single institution so that it may be susceptible to bias. Second, the lack of multicenter external validation restricts the model's applicability to other cohorts. Third, though the sample size is relatively large, it remains limited. Therefore, further large-scale, prospective, multicenter studies are necessary for optimizing and externally validating the model.

Conclusions

This study used lasso regression analysis to screen 11 variables, selected from those identified as significant in the univariate analysis of the training set. These variables were then incorporated into seven distinct machine learning algorithms to construct a predictive model (MLP, SVM, DT, AdaBoost, XGBoost, GNB, and LR). Following a thorough evaluation, which included an assessment of the AUC, DCA, and calibration curves, the XGBoost model was identified as the most optimal, demonstrating robust diagnostic performance. Furthermore, SHAP scores were calculated to determine the relative importance of features within the model. This study represents the first instance of employing a machine learning model to predict urinary infection stones based on CT values. The XGBoost model

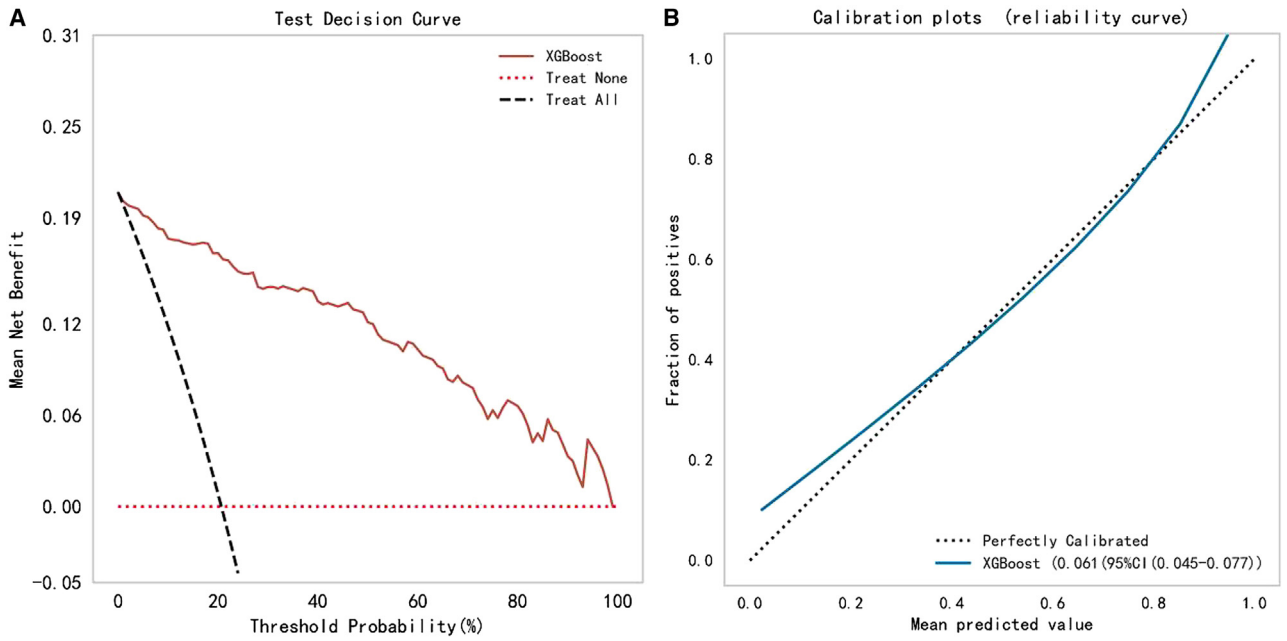

Figure 5. XGBoost model comprehensive analysis

(A) DCA curve of the XGBoost model for the validation set. The red dashed line represents the net benefit of not taking the intervention at each threshold probability, the black dashed line represents the net benefit of always taking the intervention, and the remaining solid line represents the XGBoost model.

(B) Calibration curve of the XGBoost model for the validation set. The horizontal coordinate is the average predicted probability, the vertical coordinate is the actual probability of occurrence, and the diagonal dashed line is the reference line, i.e., the case where the predicted value is equal to the actual value. The blue smooth solid line is the fitted line of the XGBoost model. The closer the fitted line is to the reference line, the smaller the value in brackets and the more accurate the model prediction.

can promptly identify infection stones before surgery, showing commendable predictive accuracy. These findings are expected to enhance the understanding of urologists in the management of infection stones, potentially leading to improved patient outcomes and more efficient clinical interventions.

RESOURCE AVAILABILITY

Lead contact

Further information and requests for resources should be directed to and will be fulfilled by the lead contact, X.X. (xixiaoqing500@sina.com) and Y.H. (273895819@qq.com).

MATERIALS AVAILABILITY

This study did not generate new unique reagents.

Data and code availability

- All data and code reported in this paper will be shared by the lead contact upon request.
- This paper does not report the original code.
- Any additional information required to reanalyze the data reported in this paper is available from the lead contact upon request.

ACKNOWLEDGMENTS

We thank all participants for taking part in this study. This work was supported by grants from National Natural Science Foundation of China (No. 82260140).

AUTHOR CONTRIBUTIONS

J.L.: Conceptualization, Methodology, Investigation, Formal Analysis, Writing – Original Draft; Y.D.: Software, Methodology; G.H.: Investigation, Writing – Original Draft; C.Z.: Data Curation; Z.Y.: Investigation; J.Z.: Software, Methodology; X.X.: Visualization, Validation, Writing – Review and Editing; Y.H.: Visualization, Writing - Review and Editing.

DECLARATION OF INTERESTS

The authors declare that there is no conflict of interest.

STAR★METHODS

Detailed methods are provided in the online version of this paper and include the following:

- KEY RESOURCES TABLE
- EXPERIMENTAL MODEL AND STUDY PARTICIPANT DETAILS
- METHOD DETAILS
  - Data collection and data preprocessing
  - Selection of predictors
  - Model development
  - Evaluation of model performance
  - Visualization of predictors
- QUANTIFICATION AND STATISTICAL ANALYSIS

SUPPLEMENTAL INFORMATION

Supplemental information can be found online at https://doi.org/10.1016/j.isci.2024.110843.

Received: March 27, 2024
Revised: May 24, 2024
Accepted: August 26, 2024
Published: October 23, 2024

REFERENCES

1. Liu, Y., Chen, Y., Liao, B., Luo, D., Wang, K., Li, H., and Zeng, G. (2018). Epidemiology of urolithiasis in Asia. Asian J. Urol. *5*, 205–214. https://doi.org/10.1016/j.ajur.2018.08.007.
2. Flannigan, R., Choy, W.H., Chew, B., and Lange, D. (2014). Renal struvite stones–pathogenesis, microbiology, and management strategies. Nat. Rev. Urol. *11*, 333–341. https://doi.org/10.1038/nrurol.2014.99.
3. Bichler, K.H., Eipper, E., Naber, K., Braun, V., Zimmermann, R., and Lahme, S. (2002). Urinary infection stones. Int. J. Antimicrob. Agents *19*, 488–498. https://doi.org/10.1016/s0924-8579(02)00088-2.
4. Koras, O., Bozkurt, I.H., Yonguc, T., Degirmenci, T., Arslan, B., Gunlusoy, B., Aydogdu, O., and Minareci, S. (2015). Risk factors for postoperative infectious complications following percutaneous nephrolithotomy: a prospective clinical study. Urolithiasis *43*, 55–60. https://doi.org/10.1007/s00240-014-0730-8.
5. Gonzalez, R.D., Whiting, B.M., and Canales, B.K. (2012). The history of kidney stone dissolution therapy: 50 years of optimism and frustration with renacidin. J. Endourol. *26*, 110–118. https://doi.org/10.1089/end.2011.0380.
6. Daudon, M., Doré, J.C., Jungers, P., and Lacour, B. (2004). Changes in stone composition according to age and gender of patients: a multivariate epidemiological approach. Urol. Res. *32*, 241–247. https://doi.org/10.1007/s00240-004-0421-y.
7. Espinosa-Ortiz, E.J., Eisner, B.H., Lange, D., and Gerlach, R. (2019). Current insights into the mechanisms and management of infection stones. Nat. Rev. Urol. *16*, 35–53. https://doi.org/10.1038/s41585-018-0120-z.
8. Stasinou, T., Bourdoumis, A., and Masood, J. (2017). Forming a stone in pelviureteric junction obstruction: Cause or effect? Int. Braz J. Urol. *43*, 13–19. https://doi.org/10.1590/s1677-5538.Ibju.2015.0515.
9. Zhu, C., Xu, Z., Gu, Y., Zheng, S., Sun, X., Cao, J., Song, B., Jin, J., Liu, Y., Wen, X., et al. (2022). Prediction of post-stroke urinary tract infection risk in immobile patients using machine learning: an observational cohort study. J. Hosp. Infect. *122*, 96–107. https://doi.org/10.1016/j.jhin.2022.01.002.
10. Motley, G., Dalrymple, N., Keesling, C., Fischer, J., and Harmon, W. (2001). Hounsfield unit density in the determination of urinary stone composition. Urology *58*, 170–173. https://doi.org/10.1016/s0090-4295(01)01115-3.
11. Marchini, G.S., Gebreselassie, S., Liu, X., Pynadath, C., Snyder, G., and Monga, M. (2013). Absolute Hounsfield unit measurement on noncontrast computed tomography cannot accurately predict struvite stone composition. J. Endourol. *27*, 162–167. https://doi.org/10.1089/end.2012.0470.
12. Alkadri, S., Ledwos, N., Mirchi, N., Reich, A., Yilmaz, R., Driscoll, M., and Del Maestro, R.F. (2021). Utilizing a multilayer perceptron artificial neural network to assess a virtual reality surgical procedure. Comput. Biol. Med. *136*, 104770. https://doi.org/10.1016/j.compbiomed.2021.104770.
13. Stidham, R.W., and Takenaka, K. (2022). Artificial Intelligence for Disease Assessment in Inflammatory Bowel Disease: How Will it Change Our Practice? Gastroenterology *162*, 1493–1506. https://doi.org/10.1053/j.gastro.2021.12.238.
14. Kalafi, E.Y., Nor, N.A.M., Taib, N.A., Ganggayah, M.D., Town, C., and Dhillon, S.K. (2019). Machine Learning and Deep Learning Approaches in Breast Cancer Survival Prediction Using Clinical Data. Folia Biol. *65*, 212–220.
15. Barah, M., and Mehrotra, S. (2021). Predicting Kidney Discard Using Machine Learning. Transplantation *105*, 2054–2071. https://doi.org/10.1097/TP.0000000000003620.
16. Griffis, J.C., Allendorfer, J.B., and Szaflarski, J.P. (2016). Voxel-based Gaussian naïve Bayes classification of ischemic stroke lesions in individual T1-weighted MRI scans. J. Neurosci. Methods *257*, 97–108. https://doi.org/10.1016/j.jneumeth.2015.09.019.
17. Rodman, J.S. (1999). Struvite stones. Nephron *81*, 50–59. https://doi.org/10.1159/000046299.
18. Beck, E.M., and Riehle, R.A., Jr. (1991). The fate of residual fragments after extracorporeal shock wave lithotripsy monotherapy of infection stones. J. Urol. *145*, 6–10. https://doi.org/10.1016/s0022-5347(17)38230-7.
19. Singh, M., Chapman, R., Tresidder, G.C., and Blandy, J. (1973). The fate of the unoperated staghorn calculus. Br. J. Urol. *45*, 581–585. https://doi.org/10.1111/j.1464-410x.1973.tb12226.x.
20. Priestley, J.T., and Dunn, J.H. (1949). Branched renal calculi. J. Urol. *61*, 194–203. https://doi.org/10.1016/s0022-5347(17)69052-9.
21. Gutierrez, J., Smith, A., Geavlete, P., Shah, H., Kural, A.R., de Sio, M., Amón Sesmero, J.H., Hoznek, A., and de la Rosette, J.; CROES PCNL Study Group (2013). Urinary tract infections and post-operative fever in percutaneous nephrolithotomy. World J. Urol. *31*, 1135–1140. https://doi.org/10.1007/s00345-012-0836-y.
22. Liu, Y.Q., Lu, J., Hao, Y.C., Xiao, C.L., and Ma, L.L. (2018). [Predicting model based on risk factors for urosepsis after percutaneous nephrolithotomy]. Beijing da xue xue bao Yi xue ban = Journal of Peking University Health sciences *50*, 507–513.
23. Martínez-Piñeiro, J.A., de Iriarte, E.G., and Armero, A.H. (1982). The problem of recurrences and infection after surgical removal of staghorn calculi. Eur. Urol. *8*, 94–101. https://doi.org/10.1159/000473488.
24. Harmon, W.J., Sershon, P.D., Blute, M.L., Patterson, D.E., and Segura, J.W. (1997). Ureteroscopy: current practice and long-term complications. J. Urol. *157*, 28–32. https://doi.org/10.1016/s0022-5347(01)65272-8.
25. Ringdén, I., and Tiselius, H.G. (2007). Composition and clinically determined hardness of urinary tract stones. Scand. J. Urol. Nephrol. *41*, 316–323. https://doi.org/10.1080/00365590601154551.
26. Piechota, J., Prywer, J., and Torzewska, A. (2012). Ab initio predictions of structural and elastic properties of struvite: contribution to urinary stone research. Comput. Methods Biomech. Biomed. Engin. *15*, 1329–1336. https://doi.org/10.1080/10255842.2011.593175.
27. Griffith, D.P., Gleeson, M.J., Lee, H., Longuet, R., Deman, E., and Earle, N. (1991). Randomized, double-blind trial of Lithostat (acetohydroxamic acid) in the palliative treatment of infection-induced urinary calculi. Eur. Urol. *20*, 243–247. https://doi.org/10.1159/000471707.
28. Kulkarni, N.M., Eisner, B.H., Pinho, D.F., Joshi, M.C., Kambadakone, A.R., and Sahani, D.V. (2013). Determination of renal stone composition in phantom and patients using single-source dual-energy computed tomography. J. Comput. Assist. Tomogr. *37*, 37–45. https://doi.org/10.1097/RCT.0b013e3182720f66.
29. Iqbal, M.W., Youssef, R.F., Neisius, A., Kuntz, N., Hanna, J., Ferrandino, M.N., Preminger, G.M., and Lipkin, M.E. (2016). Contemporary Management of Struvite Stones Using Combined Endourologic and Medical Treatment: Predictors of Unfavorable Clinical Outcome. J. Endourol. *30*, 771–777. https://doi.org/10.1089/end.2013.0257.
30. Miano, R., Germani, S., and Vespasiani, G. (2007). Stones and urinary tract infections. Urol. Int. *79*, 32–36. https://doi.org/10.1159/000104439.
31. Terry, R.S., and Preminger, G.M. (2020). Metabolic evaluation and medical management of staghorn calculi. Asian J. Urol. *7*, 122–129. https://doi.org/10.1016/j.ajur.2019.12.007.
32. Nevo, A., Golomb, D., Lifshitz, D., and Yahav, D. (2019). Predicting the risk of sepsis and causative organisms following urinary stones removal using urinary versus stone and stent cultures. Eur. J. Clin. Microbiol. Infect. Dis. *38*, 1313–1318. https://doi.org/10.1007/s10096-019-03555-6.
33. Ryan, F., Ho, C.W., Ben, C., and Dirk, L. (2014). Renal struvite stones–pathogenesis, microbiology, and management strategies. J Nat. Rev. Urol. *11*, 333–341.
34. Gadalla, A.A.H., Friberg, I.M., Kift-Morgan, A., Zhang, J., Eberl, M., Topley, N., Weeks, I., Cuff, S., Wootton, M., Gal, M., et al. (2019). Identification of clinical and urine biomarkers for uncomplicated urinary tract infection

using machine learning algorithms. Sci. Rep. *9*, 19694. https://doi.org/10.1038/s41598-019-55523-x.

35. Prywer, J., Sadowski, R.R., and Torzewska, A. (2015). Aggregation of Struvite, Carbonate Apatite, and Proteus mirabilis as a Key Factor of Infectious Urinary Stone Formation. Cryst. Growth Des. *15*, 1446–1451.
36. Resnick, M.I. (1981). Evaluation and management of infection stones. Urol. Clin. North Am. *8*, 265–276.
37. Lieske, J.C., de la Vega, L.S.P., Gettman, M.T., Slezak, J.M., Bergstralh, E.J., Melton, L.J., 3rd, and Leibson, C.L. (2006). Diabetes mellitus and the risk of urinary tract stones: a population-based case-control study. Am. J. Kidney Dis. *48*, 897–904. https://doi.org/10.1053/j.ajkd.2006.09.002.
38. Knoll, T., Schubert, A.B., Fahlenkamp, D., Leusmann, D.B., Wendt-Nordahl, G., and Schubert, G. (2011). Urolithiasis through the ages: data on more than 200,000 urinary stone analyses. J. Urol. *185*, 1304–1311. https://doi.org/10.1016/j.juro.2010.11.073.
39. Talati, V.M., Soares, R.M.O., Khambati, A., Nadler, R.B., and Perry, K.T., Jr. (2020). Trends in urinary calculi composition from 2005 to 2015: a single tertiary center study. Urolithiasis *48*, 305–311. https://doi.org/10.1007/s00240-019-01151-z.
40. Wu, Y., Mo, Q., Xie, Y., Zhang, J., Jiang, S., Guan, J., Qu, C., Wu, R., and Mo, C. (2023). A retrospective study using machine learning to develop predictive model to identify urinary infection stones in vivo. Urolithiasis *51*, 84. https://doi.org/10.1007/s00240-023-01457-z.
41. Chen, T., Zhang, Y., Dou, Q., Zheng, X., Wang, F., Zou, J., and Jia, R. (2022). Machine Learning-Assisted Preoperative Diagnosis of Infection Stones in Urolithiasis Patients. J. Endourol. *36*, 1091–1098. https://doi.org/10.1089/end.2021.0783.
42. Shen, J., Xiao, Z., Wang, X., and Zhao, Y. (2024). A nomogram clinical prediction model for predicting urinary infection stones: development and validation in a retrospective study. World J. Urol. *42*, 211. https://doi.org/10.1007/s00345-024-04904-7.
43. Liu, M., Cui, Z., Zhu, Z., Gao, M., Chen, J., Zeng, F., He, C., and Chen, H. (2022). Development of a Nomogram Predicting the Infection Stones in Kidney for Better Clinical Management: A Retrospective Study. J. Endourol. *36*, 947–953. https://doi.org/10.1089/end.2021.0735.
44. Tiselius, H.G., and Andersson, A. (2003). Stone burden in an average Swedish population of stone formers requiring active stone removal: how can the stone size be estimated in the clinical routine? Eur. Urol. *43*, 275–281. https://doi.org/10.1016/s0302-2838(03)00006-x.

STAR★METHODS

KEY RESOURCES TABLE

REAGENT or RESOURCE	SOURCE	IDENTIFIER
Deposited Data		
Raw urinary stones CT data	This paper	N/A
Software and Algorithms		
R version_4.3.2	R CRAN	https://cran.r-project.org/
Python_3.11.4	Python Software	https://www.python.org/
XGBoost _1.7.7.1	R CRAN	https://cran.r-project.org/web/packages/xgboost/
glmnet_4.1–8	R CRAN	https://cran.r-project.org/web/packages/glmnet/
pROC_1.18.5	R CRAN	https://cran.r-project.org/web/packages/pROC/
PRROC_1.3.1	R CRAN	https://cran.r-project.org/web/packages/PRROC/
caret_6.0–94	R CRAN	https://cran.r-project.org/web/packages/caret/
shapviz_0.9.3	R CRAN	https://cran.r-project.org/web/packages/shapviz/
ggplot2_3.5.1	R CRAN	https://cran.r-project.org/web/packages/ggplot2/
extrafont_0.19	R CRAN	https://cran.r-project.org/web/packages/extrafont/
RandomizedSearchCV_0.14	Scikit-learn	sklearn.model_selection.RandomizedSearchCV — scikit-learn 1.4.2 documentation

EXPERIMENTAL MODEL AND STUDY PARTICIPANT DETAILS

A total of 1413 patients who were admitted to the Second Affiliated Hospital of Nanchang University for surgical removal of urinary tract stones (percutaneous nephrolithotripsy, ureteroscopic lithotripsy, or cystoscopic lithotripsy) from February 2021 to September 2023 were selected as study subjects. All these patients are of East Asian descent. The inclusion criteria were as follows: (1) all subjects underwent a CT scan to confirm the diagnosis of urinary stones before surgical lithotripsy; (2) availability of complete medical records and relevant laboratory test results; (3) postoperative stone samples were obtained and analyzed using infrared spectrometry (infrared spectroscopy SUN-3G intelligent stone analysis system) to determine the composition of the stones. The exclusion criteria were: (1) absence of a CT scan; (2) refusal of stone composition analysis; (3) incomplete medical records or relevant examinations. Based on these criteria, 1209 eligible patients were included in the modeling.

METHOD DETAILS

Data collection and data preprocessing

The clinical data of patients were retrospectively collected, including 31 indicators such as CT values, age, gender, body mass index, presence of diabetes mellitus, hypertension, urinalysis results, and urine culture. Urine samples for analysis were obtained within 24 h of admission, while urine culture samples were taken from midstream urine within a week before surgery. A positive urine culture was defined as a single pathogen colony count exceeding 10^5/mL of urine. Urease-producing bacteria, such as Proteus mirabilis, Klebsiella pneumoniae, and Pseudomonas aeruginosa, are highly correlated with the formation of infection stones.

The composition of stones from the patients collected post-surgery, was analyzed using the LIIR-20 infrared spectroscopy automated analysis system (Tianjin Lammertech) (Figure S1). Urinary stones were categorized into four groups based on their main component (>50%): calcium oxalate stones (including calcium oxalate monohydrate and calcium oxalate dihydrate), infection stones (including struvite, carbonate apatite, and ammonium urate), uric acid stones, and calcium phosphate stones. Infection stones were further divided into two categories based on composition: (1) Simple infection stones, where the stone is composed of one or more of struvite, carbonate apatite, or ammonium urate ($\geq$95%); (2) Mixed infection stones, where the stone composition is predominantly struvite or carbonate apatite ($\geq$50%).

Diagnosis of urological calculi was primarily performed using a German Siemens 256-row spiral CT. The acquisition of urological CT imaging features such as CT values (Unit of measure: HU), stone load, stone location, number of stones and degree of urological hydrops were assessed by two specialist urologists. The images were processed and stored using the Picture Archiving & Communication System (PACS). To measure the CT value of the stone, the plane with the largest cross-sectional area was selected, and 50% of the area in the center of the stone was defined as the region of interest (ROI). The CT value was measured three times within the ROI and averaged. Different locations were repeatedly measured in the case of complex stones to obtain an average value (Figure S2).[43]

The stone load was calculated according to a specific formula: $\sum_{k=1}^{n}(0.785 \cdot \text{Widthmax} \cdot \text{Lengthmax})$.[44] Patients with recurrent kidney stones were defined as those with two or more ipsilateral kidney stone findings.

Selection of predictors

Initially, all case samples were randomly split into a training set (70%) and a validation set (30%) to aid in model development and evaluation. A total of thirty-one variables were extracted from the participants' clinical, imaging, and laboratory data. Variables with excessive missing values, such as C-reactive protein and squamous epithelial cells, were excluded. One-way analyses of variance were exclusively conducted on the training set. Variables showing statistical significance ($p < 0.05$) were subjected to Lasso regression for further screening. The rationale behind screening variables exclusively within the training set is to ensure the integrity of the dataset division, simulating the model's performance on unseen data and accurately assessing its generalization capabilities. Screening variables on the entire dataset risks 'leakage' of information from the validation set, potentially compromising the reliability of model performance assessment. The 11 variables identified from the Lasso regression analysis were utilized in seven machine learning algorithms: MLP, SVM, DT, AdaBoost, XGBoost, GNB, and LR to construct predictive models.

Model development

For each model, the RandomizedSearchCV class in the scikit-learn library was used to perform a random search to set the machine learning parameters. Random search identifies the optimal model parameters by randomly selecting combinations within a given parameter space. This method allows for quickly finding the optimal parameter combination among numerous possibilities, thereby enhancing the model's performance. To avoid overfitting, we evaluated each model's performance under each criterion through 10-fold cross-validation. Our model aims to identify patients with infection stones preoperatively and guide clinicians to early and appropriate intervention and treatment, thereby improving patient outcomes and quality of life and reducing recurrence.

Evaluation of model performance

ROC curves were generated for the seven predictive models to assess their ability to discriminate between infection and non-infection stones using the AUC. Sensitivity, specificity, PPV, NPV, accuracy, and F1 scores were also computed to comprehensively evaluate the models' performance. The threshold for model performance characteristics is determined based on the Youden Index. The model calculates a threshold using the Youden Index during each training session, and the final threshold is determined based on the optimal model.

Due to the sample imbalance, where only 19.9% (241 patients) had infected stones, Precision-Recall (PR) curves were plotted to better evaluate model performance in imbalanced datasets. The AUPR provides valuable insights for model evaluation. Additionally, decision curve analysis (DCA) and calibration curves were used to assess the diagnostic performance of the final model. These analytical techniques enhance the robustness and reliability of the model's predictive capabilities, facilitating informed clinical decision-making processes within the domain of urology.

Visualization of predictors

SHAP scores were computed to determine the significance of each variable integrated into the modeling procedure. This measure improves the transparency and interpretability of machine learning models, reducing the inherent "black box" characteristics associated with such methodologies.

QUANTIFICATION AND STATISTICAL ANALYSIS

Statistical analyses were conducted using SPSS 26.0 software. The Shapiro-Wilk test was applied to assess the normality of distributions. Quantitative data were presented as mean ± standard deviation (mean ± SD); t-tests were used for normal distributions, while the Mann-Whitney U test was used for non-normal distributions. Count data were represented as percentages, with group differences evaluated through the chi-squared or Fisher exact tests. A two-tailed p-value <0.05 indicated statistical significance. Statistical analyses were carried out using R version 4.2.3 and Python version 3.11.4.